Defense Technical Information Center Compilation Part Notice

ADP011167

TITLE: An Investigation of Adaptive Signal Processing Approaches to Active Combustion Control

DISTRIBUTION: Approved for public release, distribution unlimited

This paper is part of the following report:

TITLE: Active Control Technology for Enhanced Performance Operational Capabilities of Military Aircraft, Land Vehicles and Sea Vehicles [Technologies des systemes a commandes actives pour l'amelioration des performances operationnelles des aeronefs militaires, des vehicules terrestres et des vehicules maritimes]

To order the complete compilation report, use: ADA395700

The following component part numbers comprise the compilation report:
ADP011101 thru ADP011178

An Investigation of Adaptive Signal Processing Approaches to Active Combustion Control

Michael A. Vaudrey, William R. Saunders, and William T. Baumann
Virginia Polytechnic Institute and State University
Blacksburg, VA 24061-0328, USA

Introduction

There has been significant progress made in understanding dynamic models and control system designs for active control of thermoacoustic instabilities. During the past several years, there has been an increasing trend away from mostly empirical or experimentally-based *active combustion control* (ACC) methods in exchange for control systems that rely on more accurate understanding of the dynamic processes involved in the thermoacoustic limit cycling response. Early demonstrations of phase-shifting ACC designs (Gutmark et al., 1993; McManus et al., 1990) relied simply on a measurement of the acoustic pressure and actuation of the unsteady heat release after appropriate delay (i.e. phase shift) relative to the measured pressure signal. The phase-shifting controllers proved to be effective in many situations but were plagued by inadequate knowledge of how to predict the required phase, and gain, of the controller for varying operating conditions of the combustor. These problems naturally led to investigations of adaptive control methods.

A number of ACC researchers recognized that adaptive signal processing methods offered a possible alternative to the manually-tuned, phase-shifting controller. These adaptive filtering methods, such as the LMS algorithm proposed by Widrow and Stearns (1985), had been highly successful in the active noise and vibration control community for narrowband disturbance rejection. The most relevant application of LMS control for noise or vibration control was the so-called Filtered-U algorithm (Kuo and Morgan, 1995) which required feedback compensation for the reference sensor. The ACC implementation is similar in its need for compensation because the reference sensor is identical to the error sensor. A limited number of combustion researchers investigated the usefulness of these LMS algorithms for ACC (Billoud et al., 1992; Kemal and Bowman, 1995; Mohanraj, 1998, Annaswamy et al., 1998, and Koshigoe, 1999). However, most of the results from those experiments and numerical simulations indicated an unacceptable degree of uncertainty about the stability of the LMS-based adaptive controllers. The literature shows that the LMS controllers often seemed to promote the occurrence of peaks of unknown origin, or apparent divergence of the controllers, sometimes occurring minutes after the combustors' pressure signatures seemed to have been reduced to acceptable levels. Explanations for such behaviors have been attempted, in part, but it was recently stated that more research would be required before this class of adaptive controllers might be used reliably (Mohanraj, 1998).

This paper extends the existing research into the design of LMS adaptive filters for suppression of thermoacoustic instabilities. Through detailed numerical simulations, supported by relevant experiments on a simple tube combustor, we provide one possible method for achieving stabilizing control using an adaptive feedback architecture. As discussed by Annaswamy et al. (1998), previous researchers have not been able to avoid divergence of the LMS adaptive schemes in most cases where it has been tested. The reasons for the divergent behavior have not been made clear, but most often there have been remarks made about the stability of the gradient search algorithm or stability of the IIR filter structures that have been used for some implementations. In this paper, we carefully distinguish between two fundamental modes of instability that may be responsible for the aberrant behaviors reported by previous researchers. The first mode is related to the generation of feedback instabilities that can arise as the adaptive filter converges to the optimal solution. The second mode is related to convergence of the gradient search algorithm, analogous to the convergence issues that have been presented by Elliott et. al. (1987) for Filtered-X or Wang and Ren (1999) for Filtered-U. The primary focus of this paper is on the feedback-related instability mode as it appears to be most dominant and may be directly related to the selection of system identification method used for the adaptive filter implementation. Previous researchers have struggled with how to conduct the system identification task that is required for the LMS algorithm for this ACC application.

The key result of this paper is a description of an ACC experiment on a tube combustor that demonstrates a repeatable, stable implementation of a LMS adaptive filter controller for suppression of a limit cycling oscillation. A system identification method is proposed that results in identification of a stable plant model suitable for control of the unstable combustion oscillation. A nonlinear analysis of the system identification technique indicates that this approach, first reported by Saunders et al. (1999-2), offers advantages for adaptive filtering controllers also. Nonlinear simulations of the ACC experiment are used to

Paper presented at the RTO AVT Symposium on "Active Control Technology for Enhanced Performance Operational Capabilities of Military Aircraft, Land Vehicles and Sea Vehicles", held in Braunschweig, Germany, 8-11 May 2000, and published in RTO MP-051.

explain the detailed behavior of the plant for those cases where control is achieved. Additionally, we propose plausible explanations for the source of unstable applications of the LMS controller (observed mostly for higher equivalence ratios in this research) although the detailed proof for those explanations is left for future work.

The paper is organized as follows. The following section introduces several different adaptive filter architectures that must be understood to appreciate LMS control of combustion oscillations. A stable system, subject to an exogenous disturbance, is used to illustrate the key issues that arise when the error signal must also serve as the reference signal input to the adaptive filter and LMS weight update equation. Then, a self-excited system is investigated to show the differences between controlling the effects of a disturbance on a stable plant and suppressing the unstable, limit cycling system response of the self-excited system. The system ID method used for the adaptive filter is introduced and supported using describing function arguments. In Section 3, simulations and experiments for a tube combustor (Saunders et al., 1999-1) are presented and compared. It is shown that there appears to be a range of operating conditions that the adaptive filter can predictably control based on the system identification method chosen for the work. A comparison between simulations and experiments reveals identical behaviors and will form the basis for more detailed future studies. Section 4 provides the concluding remarks.

Adaptive Feedback Control

Classical Disturbance Suppression

The adaptive feedback control considered in this paper can be viewed as a special case of Filtered-U control where the control-to-reference path and the control-to-error path are identical because the error sensor also serves as the reference sensor (Kuo and Morgan, 1996). Figure 1 shows the adaptive feedback control block diagram for the case of an external disturbance (completely unrelated to a self-excited limit cycle). It is instructive to briefly examine this system as a precursor to controlling the self-excited system.

In a purely feedforward control system, a separate reference signal that is correlated with the disturbance is used as the input to the adaptive filter and it is well-known that correct estimation of the dynamic phase, within ninety degrees, is sufficient to prevent divergence of the LMS gradient search (Elliott et al., 1987). In adaptive feedback control, the reference signal is derived directly from the error sensor by removing the component of the error signal that is due to the control signal, leaving only a measure of the disturbance. If we let the control signal be the output of the FIR adaptive filter (W), we note that it must go through the plant dynamics (G_p) before acting on the external disturbance (n). The dynamics represented by the plant will include everything present in the control signal-to-error signal path, including the A/D and D/A. Therefore, removing the component of control from the error requires subtracting the output of the adaptive filter, filtered by the plant estimate, from the measured error signal. Therefore, if the plant estimate is not perfect, a non-zero feedback path is introduced. The closed loop transfer function between the error and the disturbance can then be written as:

$$\frac{e}{n} = \frac{1 + \hat{G}_p W}{1 + \hat{G}_p W - G_p W} \qquad [1]$$

Unlike the self-excited system (discussed shortly), if the plant estimate is exact (i.e. $G_p = \hat{G}_p$), there is no feedback loop (the denominator of the above transfer function vanishes) and the system behaves as a strictly feedforward system where $\hat{G}_p$ and W are both stable systems. For the case where $G_p \neq \hat{G}_p$, it is clear that the poles of Equation 1 will change with the adaptation of the filter W and no guarantees are made concerning system stability. This is the first mode of instability that may exist in the adaptive feedback design, and is easily analyzed using Bode or Nyquist gain and phase relationships for the loop gain:

$$\frac{G_p W}{1 + \hat{G}_p W} \qquad [2]$$

In adaptive feedforward systems such as Filtered-X control, algorithm divergence can result when the step size of the update equation is too large, or when there is a phase error in the plant estimate greater than 90°. A similar analysis is much more difficult for the adaptive feedback case but has been discussed by (Wang and Ren, 1999). Their convergence result requires a strictly positive real assumption on a transfer function that depends on the unknown plant. Thus, it is of limited applicability for many real world

problems. The adaptive feedback weight update shown in Equation 3 clearly illustrates nonlinear characteristics, indicating that the 90° rule for the Filtered-X algorithm is not necessarily applicable to this problem.

$$w(k+1) = w(k) + \mu(\hat{G}_p n + \hat{G}_p G_p c - \hat{G}_p \hat{G}_p c)(-n - G_p c) \quad [3]$$

Our ongoing research in adaptive filtering methods for ACC has shown that the dominant instability mode is not related to algorithm divergence. The following simulation results for an adaptive feedback system illustrate an occurrence of a feedback loop instability; however, the ID error does not result in a divergence of the algorithm. The plant shown in Figure 1 was chosen to have unity magnitude and linear delay while the plant estimate was chosen as the same system with a different linear delay. The difference in phase between the plant and estimate increased almost linearly, reaching an excess of 1000° of phase error by 1000 Hz, thus ensuring the possibility for divergence of the weights due to an inaccurate system identification. Figure 2 illustrates the uncontrolled and controlled power spectra of the disturbance at 40 Hz. Initially, the tone is suppressed with only two adaptive filter weights but the 'out-of-band' gain that accompanies the optimal adaptive filter causes a loop instability at 810 Hz to occur as evidenced by the frequency response magnitude in excess of 0 dB at the 810 Hz phase crossover frequency. Stated otherwise, this LMS control diverges because of the feedback loop instability, NOT divergence of the algorithm. Simply increasing the number of adaptive filter weights reduces the gain of the adaptive filter at frequencies away from the disturbance, so that the filter provides sufficient gain at 40 Hz to suppress the disturbance without generating feedback loop instabilities. For this stabilizing situation, the phase error between the plant and estimate is still in excess of 90° at many frequencies but the algorithm *never* diverges. It is interesting to observe that some previous researchers have attempted to achieve control with only two-weight adaptive filters, hereby shown to destabilize the system unnecessarily. This problem is minimized for real experiments where narrow bandpass filters shape the error signal but is noteworthy, nonetheless.

If the gradient search algorithm itself is diverging due to an inaccurate identification, the increasing magnitude of the adaptive filter may also be sufficient to cause a loop instability. Likewise, the algorithm may be converging (with a certain plant error) to a solution that results in a feedback loop instability. It is impossible to completely separate the gradient search divergence from the potential loop instabilities described in the example above. Analysis of algorithm divergence is a focus of future research.

Self-Excited Systems

The existence of a feedback path, related to using the error sensor to generate the reference signal, is responsible for transforming the LMS control approach into an adaptive feedback system. As illustrated in the previous section, the feedback loop for the external disturbance adaptive feedback system (Figure 1) disappears for cases where the plant and plant estimate are identical. This is certainly desirable because one advantage of an adaptive feedforward control is its inherent stability. Unfortunately, it is not possible to eliminate the corresponding feedback path when this same adaptive control is applied to a self-excited system, as discussed next. This is one of the first important distinctions associated with applications of LMS adaptive filtering for ACC.

Figure 3 illustrates a simplified block diagram of an adaptive feedback controller applied to a self-excited system, such as the VPI tube combustor. The output of the adaptive filter is filtered by the plant estimate and is used to generate the reference signal from the error signal as before; although the plant estimate is quite different now as a result of the inclusion of the self-excited system. The control signal is altered by the plant and actuator dynamics (G_{ACT}) before generating a pressure that interacts with the pressure from the self-excited system (G_A and G_F) containing acoustic and flame dynamics. The role of the nonlinearity in the self-excited feedback loop is critical in establishing the ability to achieve a stable estimate of the plant – an important comment referring to system identification of a limit cycling system that will be discussed in detail in the following section. For now, it is possible to examine the feedback structure of the system without incorporating the nonlinearity, and assuming the self-excited system is marginally stable. The total pressure (P_T) serves as the error signal to be reduced and is used by the adaptive feedback structure to update the weights and create the reference signal. If the feedback system of Figure 3 is analyzed, the expression for the autonomous response P_T results in the following system characteristic equation:

$$1 - \frac{G_{ACT} W}{1 + \hat{G}_p W - G_A G_F - G_A G_F \hat{G}_p W} \quad [4]$$

where for a marginally stable linear system model, Equation 5 can be substituted in Equation 4 as the plant estimate.

$$\frac{P_T}{p} = \hat{G}_p = \frac{G_{ACT}}{1 - G_A G_F} \quad [5]$$

Equation 4 shows that even if the control-to-error path of Equation 5 (i.e. the probe input p to the total pressure P_T) is identified perfectly in a linear system sense, it does not guarantee that the roots of Equation 4 (poles of adaptive feedback system) will be stable. Recall that it did for the external disturbance feedback problem of Figure 1. It is also clear that the characteristic equation for LMS control of the self-excited plant has roots that depend on the self-excited system, the actuator path, and the adaptive filter.

The previous result shows that it is not possible to break the feedback loop created by the reference signal estimation when dealing with a self-excited plant. Before addressing the stabilizability of the self-excited system with the adaptive filter W, we will limit the selection of the plant estimate to only stable $\hat{G}_P$. The question still arises as to how one makes $\hat{G}_P$ a stable representation of Equation 5 when the roots of $(1-G_A G_F)$ are in the right half plane. The following section explains how the limit cycling plant *can* be accurately represented by a stable system due to the nonlinearity in the self-excited system. Previous researchers have indicated problems using a 'stable' representation of the self-excited system for the required plant estimate. However, the approach documented below has not been previously discussed as a means for acquiring a stable plant estimate $\hat{G}_P$ that accurately represents the dynamics of the limit cycling system and can ultimately be used for stabilizing control.

System Identification

The approach to identifying the open-loop plant for inclusion in the adaptive algorithm relies on a probe signal consisting of low-amplitude sinusoids at frequencies near the limit-cycle frequency and within the passband of the bandpass filter used to filter the pressure signal before control. Using a Fourier transform of the output signal, the frequency response of the plant at a small number of frequencies can be determined. Using a least-squares approach, a low-order, discrete-time model can be fit to this data and is used as the model of the plant.

Since the open-loop plant is in a steady limit cycle, it is not immediately clear whether such an identification approach will produce a reasonable linear model or whether such a model will be stable or unstable. Our experimental results have shown that very low-order linear models can account accurately for the frequency response data and that these models are always stable.

To understand this, consider the block diagram in Figure 4. From a describing function analysis, the gain of the limit cycle through the static nonlinearity is such that the total gain around the loop is unity. When a probe signal is injected into the system, we expect that the frequency response at the probe frequency will be that of the linear system made up of the linear blocks in the diagram and with the nonlinear block replaced by a suitable linear gain.

To determine the value of this gain, consider an input to the nonlinearity of the form

$$x = A_1 \sin \omega_1 t + A_2 \sin(\omega_2 t + \theta) \quad [6]$$

where ω_1 is the frequency of the limit cycle, ω_2 is the frequency of the probe and $A_1 >> A_2$. A first order approximation of the output of the nonlinearity, $f(x)$, is given by Equation 7.

$$f(A_1 \sin \omega_1 t + A_2 \sin(\omega_2 t + \theta)) = f(A_1 \sin \omega_1 t) + f'(A_1 \sin \omega_1 t) A_2 \sin(\omega_2 t + \theta) \quad [7]$$

and will be valid for A_2 sufficiently small. The gain of the nonlinearity at the limit cycle frequency is given by Equation 8.

$$\frac{2}{A_1 T} \int_0^T \left[f(A_1 \sin \omega_1 t) + f'(A_1 \sin \omega_1 t) A_2 \sin(\omega_2 t + \theta) \right] \sin \omega_1 t dt \quad [8]$$

where T is the length of a period of the overall waveform. If no period exists, then the limit as $T \to \infty$ can be taken. By arguing that the integral of incommensurate frequencies will vanish, the second term in the integral disappears and the linear gain associated with the limit cycle frequency, which is equal to the describing function of the nonlinearity, is

$$g_{LC} = \frac{2}{A_1 T} \int_0^T f(A_1 \sin \omega_1 t) \sin \omega_1 t dt \quad [9]$$

The gain of the nonlinearity at the probe frequency is given by Equation 10.

$$\frac{2}{A_2 T}\int_0^T \left[f(A_1 \sin\omega_1 t) + f'(A_1 \sin\omega_1 t)A_2 \sin(\omega_2 t+\theta)\right]\sin(\omega_2 t+\theta)dt \qquad [10]$$

Arguing as before, the first term in the integral will go to zero. In addition, the only part of the second term which will contribute to the integral is the constant component of $f'(A_1 \sin\omega_1 t)$ times the constant component of $A_2 \sin^2(\omega_2 t+\theta)$. Thus, the gain at the probe frequency is given by Equation 11.

$$g_{\Pr} = \frac{1}{T}\int_0^T f'(A_1 \sin\omega_1 t)dt \qquad [11]$$

Note that the gain of the probe signal is independent of the amplitude and frequency of the probe signal, subject to the restriction that the amplitude of the probe be small.

For the tanh nonlinearity considered in this paper, the limit-cycle and probe gains can be computed numerically and are shown in Figure 5. The gain of the probe signal is less than the gain of the limit cycle signal through the nonlinearity. Since the gain of the limit cycle frequency is just that value needed to make the closed-loop system marginally stable, the lower probe gain will cause the closed-loop system to appear stable. Since the probe gain is not a function of the probe frequency, the system identified by considering the frequency response at the probe frequency will appear linear and stable.

Analysis of Adaptive Feedback Applied to Self-Excited Systems

It is clear from the above discussion, how a linear representation of a nonlinear self-excited system can represent the measured control-to-error path if Equation 5 is re-written as

$$\frac{P_T}{p} = \hat{G}_p = \frac{G_{ACT}}{1 - G_A G_F g_{\Pr}} \qquad [12]$$

This plant estimate is stable at all probe frequencies, thereby avoiding the issue of attempting to use an unstable system identification, or a time-delay plant, as other investigations have discussed. On a related note, we point out that this system ID method also makes it possible to design a feedback controller that will apply the correct phase to the system while avoiding secondary peaks induced from the controller feedback loop (Vaudrey et al., 2000). The required gain for stabilization can be predicted only if the system gains of G_A and G_F are known, thus defining the location of the linear system poles in the right-half Laplace plane.

To summarize the issues to this point, we reiterate that Equation 12 solves only the problem of performing the system identification task for an unstable dynamic plant. There remain the issues of whether the optimal adaptive filter weights can be shown to stabilize the self-excited system, how to determine whether feedback-related instabilities (related to the plant estimate or transient adaptive filter weights) will destabilize the adaptive wideband application, and further analyses that will shed insight on the selection of a stable plant estimate $\hat{G}_P$ for use in the controller. The following discussion attempts to clarify some of these issues.

First, we examine the form of the optimal adaptive filter weights. (The reader is cautioned that the definition of the optimal adaptive filter used here is not based on the classic definition of the Wiener weights.) The self-excited adaptive feedback control system, illustrated by Figure 6, can be used to determine the optimal adaptive filter that sets the total pressure P_T of the controlled plant equal to zero. Equating the top loop to the bottom loop (with a minus sign) and solving for the optimal adaptive filter (W_{OPT}), Equation 13 results.

$$W_{opt} = \frac{-G_A G_F}{G_{ACT} + G_A G_F \hat{G}_p} \qquad [13]$$

By substituting Equation 13 into the block diagram of Figure 6 as the adaptive filter W, it is obvious that the lower loop (feedback controller) exactly cancels the upper loop $G_A G_F$ resulting in a completely stabilized closed loop system. Equation 14 illustrates this result for the probe input shown in Figure 6

$$\frac{P_T}{p} = \left.\frac{G_{ACT}(1+\hat{G}_p W)}{(1-G_A G_F)(1+\hat{G}_p W) - G_{ACT} W}\right|_{W=W_{opt}} = G_{ACT} \qquad [14]$$

Discussion of the optimal adaptive filter weights is more interesting for this self-excited plant application because of the quiescent state that the combustor will reach as soon as the poles have crossed back into the left-half Laplace plane (under the action of the controller). Because the open loop self-excited system of Equation 14 does not contain dynamics that are on the imaginary axis (i.e. marginally stable), there is a set of gains (between the imaginary axis and the optimal solution) that will stabilize the system without requiring the adaptive filter to reach the optimal solution. This system will be more lightly damped than the open loop system but still stabilized. If the adaptation causes the system to stabilize, the error signal will go to zero and the adaptation will stop, never reaching the optimal gain. **This is easily understood by recognizing that the adaptive filter solution that will ensure that the real parts of the roots of Equation 4 are all negative, is a different solution than the optimal solution of Equation 13.** The former will occur before the latter and cease adaptation as long as Equation 14 represents stable dynamics.

As mentioned earlier, there are two methods in which the adaptive wideband feedback system may not achieve stabilizing control. The first is easily identifiable as a feedback loop instability (see Equation 4), whereas the second is less well-defined as a gradient search error. The gradient search error may arise as a result of the step size parameter being too large or because the phase error of the Filtered-X control results in the LMS searching in the wrong direction on the mean-squared error performance surface. The plant estimation error analysis will be left for future work but cannot be completely separated from the feedback loop instabilities, as discussed next.

The roots of Equation 4 represent the closed loop poles of the controlled self-excited system. While it is possible to analyze each component of the system for stability in terms of gain and phase margins, it is more straightforward to insert the adaptive filter in Equation 4 to determine the closed loop root locations. It should be noted however, that because the characteristic equation is a function of the adaptive filter, an algorithm divergence will eventually result in a loop instability due to the increasing gain of the adaptive filter. It is important to distinguish between the two cases of instability by examining the convergence or divergence of the weights toward the optimal solution prior to inducing a loop instability.

It is now possible to see how the adaptive filter imparts the needed gain and phase to control the limit cycling system through the feedback loop. The significance of the control-to-error path in the controller transfer function is evident from Figure 6, which is a rearrangement of Figure 3. $\hat{G}_P$ clearly contributes to the gain and phase of the controller. However, there is another even more important issue that needs to be appreciated about the use of $\hat{G}_P$ identified by Equation 12. After inspection, it is clear that the version of $\hat{G}_P$ used during control is the correct identification of the control-to-error path *only* when the control loop is open. This important distinction is made apparent by examining the same (actual) control-to-error path *after* the control loop has been closed as shown in Figure 3. Performing the block diagram algebra, Equation 15 illustrates the new control-to-error transfer function in terms of the error signal (P_T) and the probe signal "p".

$$\frac{P_T}{p} = G_p = \frac{G_{ACT}(1+\hat{G}_p W)}{(1-G_A G_F g_{LC})(1+\hat{G}_p W) - G_{ACT} W} \qquad [15]$$

It is now obvious that after the control loop is closed and the adaptive filter grows in magnitude, its influence over the control-to-error path becomes more significant. (Note that setting W=0 in Equation 15 yields Equation 12). The fixed control-to-error path estimate $\hat{G}_P$ used in this control scheme (Equation 12) also influences the actual control-to-error path as the adaptive filter grows. Therefore, for adaptive filters requiring large magnitudes to stabilize the self-excited system, it is more likely that the actual control-to-error path will differ significantly from the fixed control-to-error path estimate obtained prior to closing the control loop.

Simulation and Experimental Results

Simulation Description

A simulation has been designed to permit rapid and easy investigation of the performance of the adaptive feedback controller in conjunction with the self-excited, limit cycling system. As will be seen, initial results from the simulation agree closely with the behavior of the actual experiment.

Figure 3 represents the general form of the adaptively controlled self-excited system that was simulated. The self-excited loop consists of a low pass filter to represent a model of the flame dynamics (G_F), a static nonlinearity represented by a hyperbolic tangent function, and a single mode lightly damped (2%) acoustical model (G_A) at approximately 175 Hz. The loop gain and nonlinearity gain were adjusted to yield a

steady limit cycle after approximately 2 seconds at a sampling rate of 1600 Hz. The actuator path consists of the acoustical model plus some amount of phase delay. For the experiment this delay represents all components in the control-to-error path.

The simulation runs in two separate modes, as does the experimental setup. After the limit cycle is established, a multi-tone probe signal is applied to the open loop plant as shown in Figure 4. The input to output relationship at the probe frequencies establishes the magnitude and phase of the linear plant as described in the system identification section above. This discrete frequency response data is then used to generate a least squares infinite impulse response (IIR) transfer function fit in the z-domain, typically of order less than 6, and always stable with a pole very near the unit circle (representing the limit cycle frequency). This fit is then used as the plant estimate during the second mode of the simulation. After the limit cycle has reached a steady state, and the probe frequencies have been turned off, the plant model mentioned above is used in the adaptive feedback control loop shown in Figure 3, both as the filtered-X part of the LMS and the plant estimate used to derive the reference signal.

The first simulation illustrated here is a case having a relatively low heat release, corresponding to a low gain in the self-excited feedback loop. Since broadband control is not the goal, only two adaptive filter weights were used to control the single tone instability. In the experimental setup, a steep (8-zero, 16-pole) bandpass filter was used to eliminate frequency content other than the limit cycle tonal. In the simulation, the only significant content in the error signal is the limit cycle sinusoid so a filter was not necessary. Using the stable plant model generated from the fit of the FRF obtained from the process shown in Figure 4, and a relatively fast convergence parameter for the LMS weight update equation, it is seen that the two adaptive weights shown in Figure 7 quickly reach a steady state condition that completely stabilizes the limit cycle as shown by the controlled and uncontrolled (dotted) power spectra in Figure 8.

As discussed in the Analysis section above, it is not required that the adaptive filter achieve the optimal gain in order to drive the error signal to zero. Figure 9 clearly illustrates this by showing the path of the magnitude and phase of the actual adaptive filter during adaptation, as compared to the optimal magnitude and phase as computed from Equation 13.

Also addressed in the analysis section was the possibility of feedback loop instabilities for the adaptive feedback system. An inaccurate plant model may contribute to causing a feedback loop instability by raising the gain near a phase crossover frequency. In order to analyze this more carefully, the frequency of the limit cycle instability (governed primarily by the frequency of the acoustic resonance) was deliberately altered while leaving the plant *model* unchanged. The frequency of the acoustic mode can shift at least 6 degrees in the negative direction while still stabilizing the system with the 175 Hz based plant model while it could only shift 4 Hz in the positive direction (to 179 Hz) before it was unable to control the system. (This would seem to imply that a plant model shifted higher in frequency would provide more robustness to changes in the plant under the action of the controller. More investigation is required in order to substantiate this theory). As shown by the power spectra in Figure 10, the instability occurred at the same frequency as the limit cycle and was predicted by the open loop Bode diagram of Figure 11 for the system of Figure 6.

While intentional creation of plant model error is instructive for tracking the source of divergence, it is not exactly true to the experiment itself. The plant changes under the action of the controller for higher heat releases, more drastically than it changes for lower heat releases. When the self-excited system is amplified to simulate higher heat release (moving the unstable pole further into the right half plane), the simulation has the same difficulties as the experiment in stabilizing the system. Figure 12 shows an upward shift in frequency of the limit cycle under the action of the control (solid trace). The time domain behavior searches between amplitudes higher and lower than the original limit cycle, unable to achieve stabilizing control because the plant model is too inaccurate when the limit cycle begins moving higher in frequency, a behavior that is amplified by the increased heat release.

Experimental Results

The experimental process was identical to that described in the simulation section above. A multi-tone FRF was performed on the entire plant and a least squares fit was applied to the data to generate an infinite impulse response filter model that represented the limit cycling plant. This model was then used in the experimental structure shown in Figure 13.

With the heat release at a relatively low gain (controlled by adjusting the equivalence ratio to a value of 0.51 and a total flow rate of 120 cc/sec), the Rijke tube combustor instability at 175 Hz was stabilized indefinitely with a two weight adaptive filter and the stable plant model obtained prior to control. Figure 14

shows (in asterisks) the actual magnitude and phase data collected from the tube with the 6th order model frequency response shown as the solid line.

Figure 15 shows the uncontrolled (dotted) and controlled power spectra of the total pressure in the tube (converted from voltage units). The second harmonic at 350 Hz disappears under control, revealing the shape of the third acoustic mode of the tube. The natural damping of the second acoustic mode is greater than that which is shown in Figure 15, but as discussed earlier, the system can be stabilized by having a pole in the left half plane that is more lightly damped than the natural acoustic mode.

A manually adjustable gain and phase shift controller was also applied to the same limit cycling system. Referring to Figure 6, it is apparent that the fixed gain controller replaces the transfer function:

$$\frac{W}{1+\hat{G}_p W} \qquad [16]$$

Examining the magnitude and phase of the converged Equation 16 at 175 Hz as compared to the magnitude and phase of the phase shifting feedback controller, it is seen in Figure 16 that the phase of both controllers is nearly the same at 175 Hz. The magnitude however is significantly lower for the adaptive system because the error signal has been driven below the 1-bit noise floor of the A/D. In addition, excessive gain was applied to the manual control system, that might have induced feedback instabilities (Vaudrey et. al. 2000, Saunders et. al. 1999-2). The adaptive controller can prevent controller induced instabilities by changing its shape and adjusting its magnitude to minimize the mean squared error.

Although no data was collected, the adaptive controller was used to control a higher equivalence ratio of 0.57 at the same total flow rate. This corresponded to the increase in gain for the simulation shown in Figure 12. The searching time domain behavior and the upward shift in frequency apparent in the simulation were both witnessed in the experimental application of the same system. While the adaptive controller was unable to completely stabilize the higher equivalence ratio system, it was able to exercise significant authority over the instability by cycling its amplitude over time, as seen in the simulation.

Conclusions

An adaptive control strategy based on the LMS algorithm was used to stabilize a limit cycling Rijke tube combustor. It was shown that a stable linear model of the nonlinear limit cycling control-to-error path can be used in an adaptive feedback arrangement to achieve the stabilizing control. It was also shown that ill-behaved controller performance is often due to unstable feedback loops caused by inaccurate plant models and large adaptive filter amplitudes required by high heat release situations. Finally, it was shown that a numerical simulation has been developed that accurately predicts the experimental performance, and can be used as a tool for designing control strategies that are effective over a broad range of operating conditions.

Previous research (Annaswamy et. al., Billoud et. al., Kemal et. al., Koshigoe et. al.) in the area of adaptive LMS control for combustion instabilities has met with limited success. Structures incorporating fixed system models of stable and unstable plants have exhibited numerical instabilities over time. This paper provides analytical, simulation, and experimental proof-of-concept for using a stable plant model for adaptive feedback control of limit cycling oscillations. In addition, a method for tracking loop instabilities that can result in spurious behavior of the adaptive feedback system has been presented.

References

Annaswamy, A.M., O.M. El Rifai, M. Fleifil, J.P. Hathout, and A.F. Ghoneim, "A Model-based Self-tuning Controller for Thermoacoustic Instability," *Combustion Science and Technology,* **135**, 1998, pp. 213-239.

Billoud, G., M.A. Galland, C.H. Huu, and S. Candel, 'Adaptive Active Control of Combustion Instabilities,' *Combust. Sci. and Tech.*, **81**, 1992, pp.257-283.

Elliott S.J., I.M. Stothers, and P.A. Nelson, 'A Multiple Error LMS Algorithm and Its Application to the Active Control of Sound and Vibration, ' *IEEE Transactions on Acoust., Speech, and Sig.Proc.*, Vol.ASSP-35, No.10, Oct., 1987.

Gutmark, E., T.P. Parr, K.J. Wilson, D.M. Hanson-Parr, and K.C. Schadow, 'Closed-loop Control in a Flame and a Dump Combustor,' *IEEE Control Systems*, **13**, 1993, pp.73-78.

Kemal, A. and C. Bowman, 'Active Adaptive Control of Combustion,' *Proceedings of the IEEE Conference on Control Applications*, 1995, pp.667-672.

Koshigoe, S., T. Komatsuzaki, and V. Yang, 'Adaptive Control of Combustion Instability with On-Line System Identification,' *Journal of Propulsion and Power*, **15**, 1999, pp.383-389.

Kuo, S.M. and D.R. Morgan, 'Active Noise Control Systems, Algorithms and DSP Implementations,' John Wiley and Sons, Inc., New York, NY, 1996.

McManus, K.R., U. Vandsburger, and C.T. Bowman, 'Combustor Performance Enhancement Using Direct Shear Layer Excitation,' *Combustion and Flame,* **82**, 1990, pp. 75-92.

Mohanraj, R. and B.T. Zinn, "Numerical Study of the Performance of Active Control Systems for Combustion Instabilities, " AIAA 98-0356, 36th Aerospace Sciences Meeting & Exhibit, Reno, NV, Jan., 1998.

Saunders, W.R., L. Nord, C.A. Fannin, X. Huang, W.T. Baumann, V. Khanna , U. Vandsburger, L. Haber, B. Eisenhower, S. Liljenberg, 'Diagnostics and Modeling of Acoustic Signatures in a Tube Combustor, *' Proceedings of the 6th Int. Congress on Sound and Vib.*, Copenhagen, Denmark, 1999-1.

Saunders, W.R., M.A. Vaudrey, and B. A. Eisenhower, U. Vandsburger, and C.A. Fannin, 'Perspectives on Linear Compensator Designs for Active Combustion Control,' AIAA 99-0717, 37th AIAA Aerospace Sciences Meeting and Exhibit, Reno, NV, Jan. 1999-2.

Vaudrey, M.A., W.R. Saunders, and B. A. Eisenhower, 'A Test-Based Methodology for Apriori Selection of Gain/Phase relationships in Proportional, Phase-Shifting Control of Combustion Instabilities,' Proceedings of ASME Turbo Expo 2000, Munich, Germany, May 2000.

Wang, A.K. and W. Ren, 'Convergence Analysis of the Filtered-U Algorithm for Active Noise Control,' *Signal Processing Journal* 73 (1999), pp.255-266.

Widrow, B. and S.D. Stearns, 'Adaptive Signal Processing,' Prentice-Hall, Inc., Englewood, N.J., 1985.

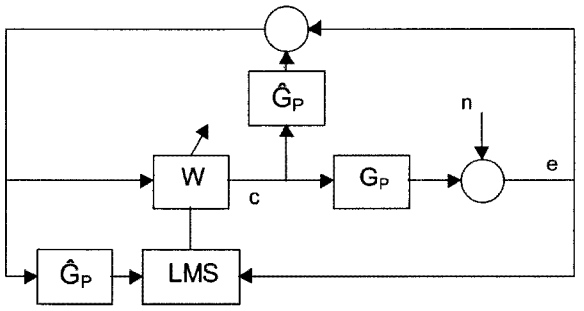

FIGURE 1: ADAPTIVE FEEDBACK EXTERNAL DISTURBANCE

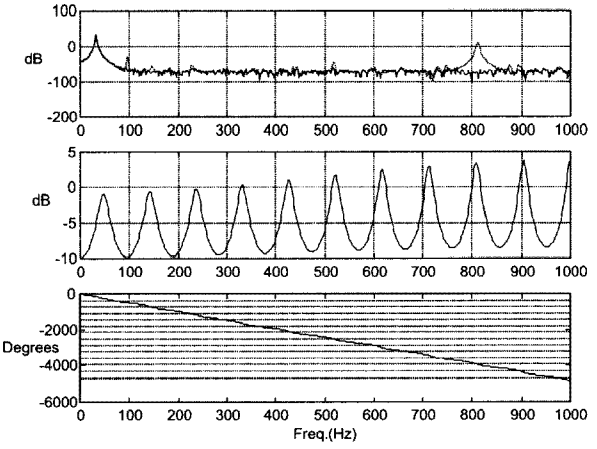

FIGURE 2: POWER SPECTRA AND OPEN LOOP FRF

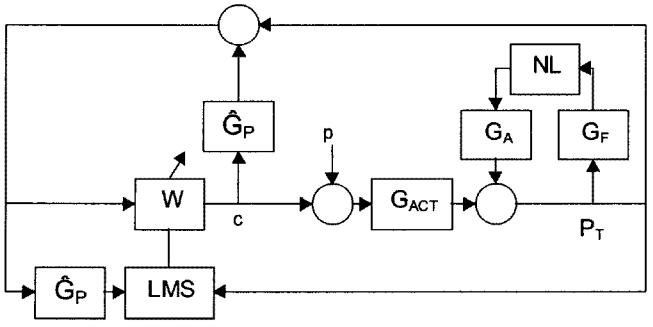

FIGURE 3: ADAPTIVE FEEDBACK SELF EXCITED

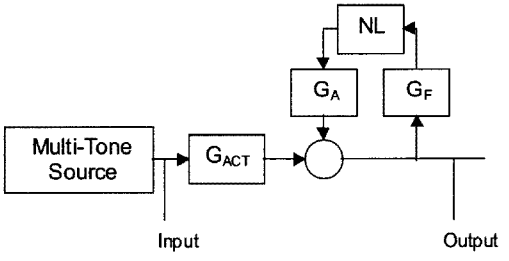

FIGURE 4: SYSTEM ID– OPEN LOOP

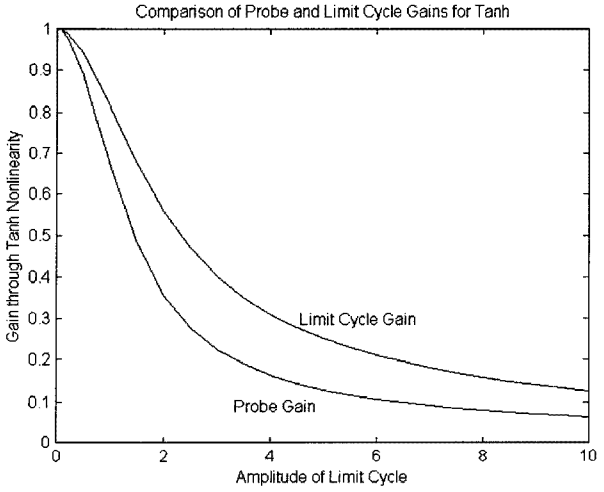

FIGURE 5: PROBE GAIN AND LIMIT CYCLE GAIN

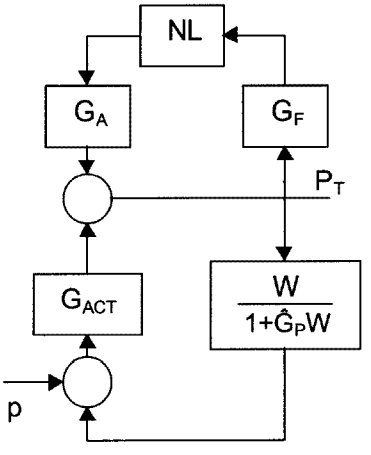

FIGURE 6: ADAPTIVE FEEDBACK SELF EXCITED

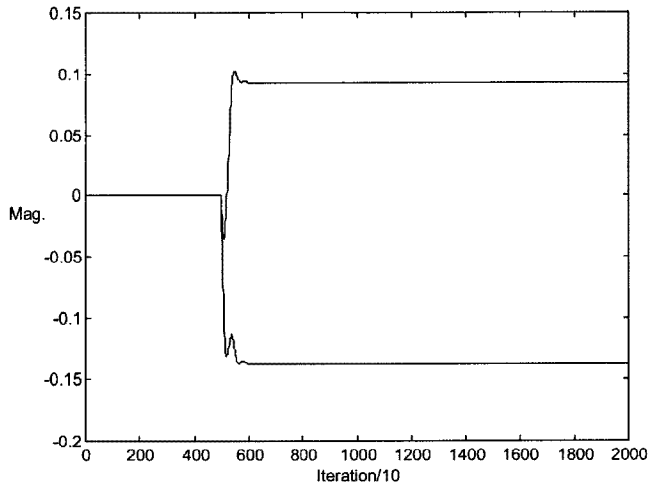

FIGURE 7: WEIGHTS IN TIME

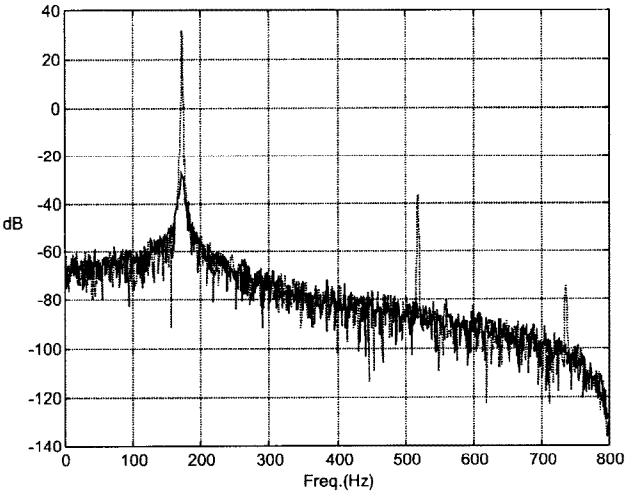

FIGURE 8: POWER SPECTRA CONTROLLED (SOLID)

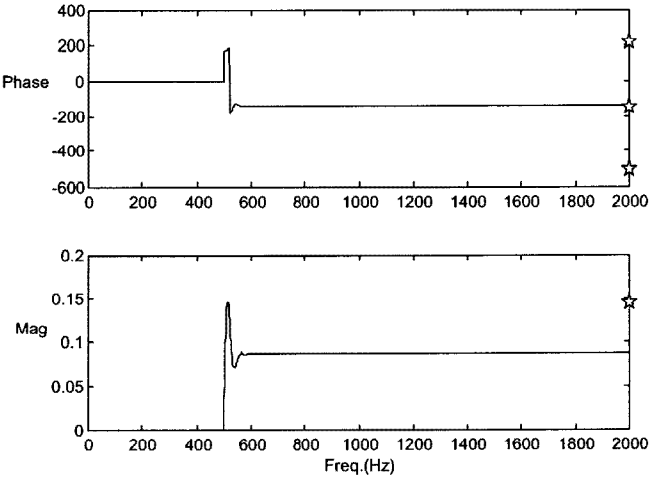

FIGURE 9: A.F. MAGNITUDE AND PHASE AT 175 HZ

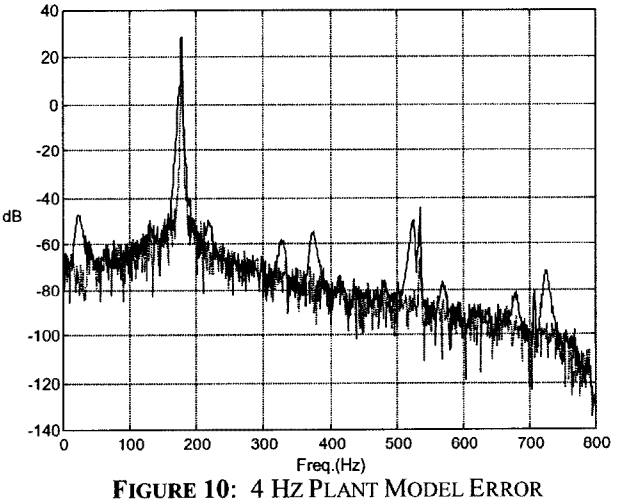

FIGURE 10: 4 HZ PLANT MODEL ERROR CONTROLLED SOLID

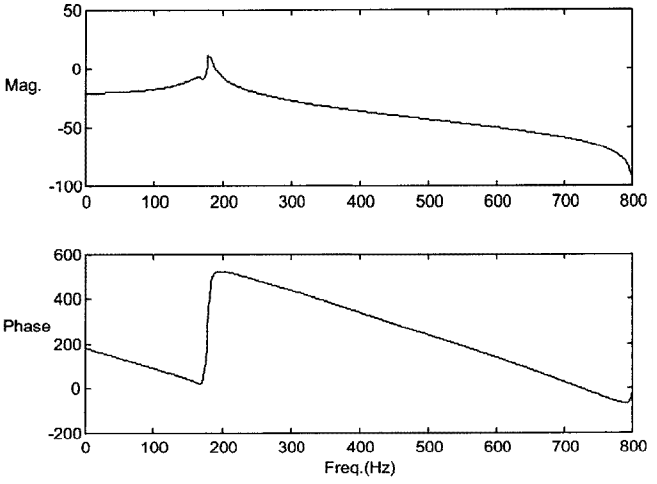

FIGURE 11: OPEN LOOP FRF – 4 HZ ERROR

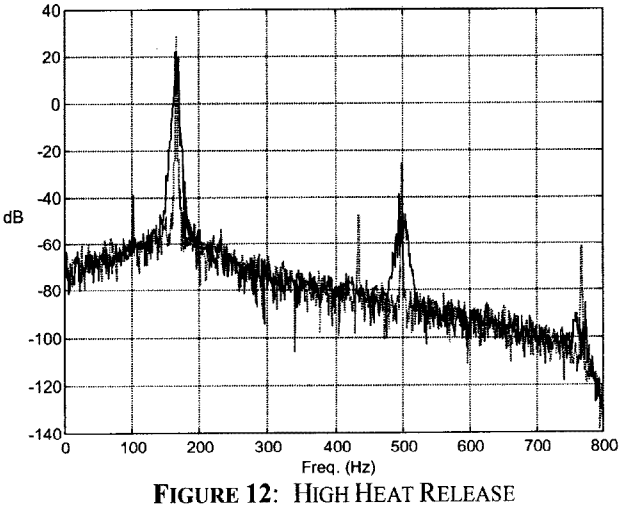

FIGURE 12: HIGH HEAT RELEASE CONTROLLED-SOLID

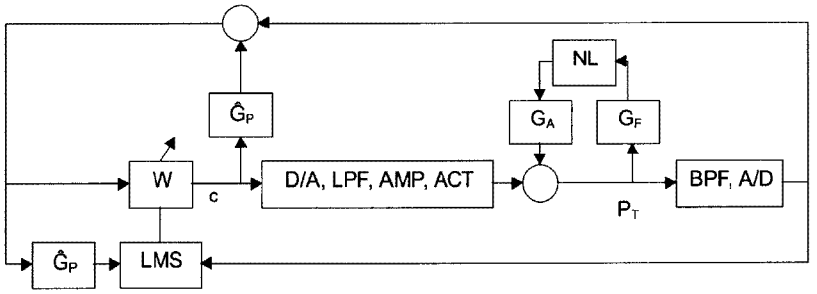

FIGURE 13: ADAPTIVE FEEDBACK EXPERIMENTAL SETUP

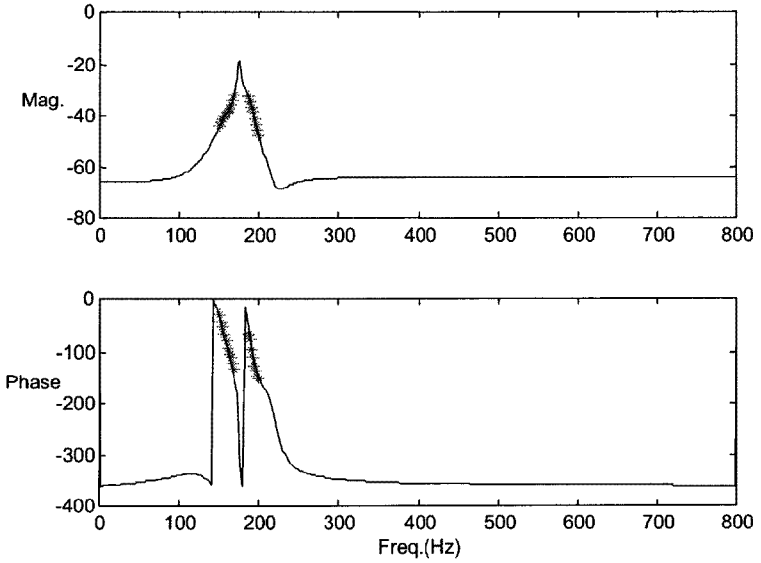

FIGURE 14: EXPERIMENTAL PLANT MODEL FIT

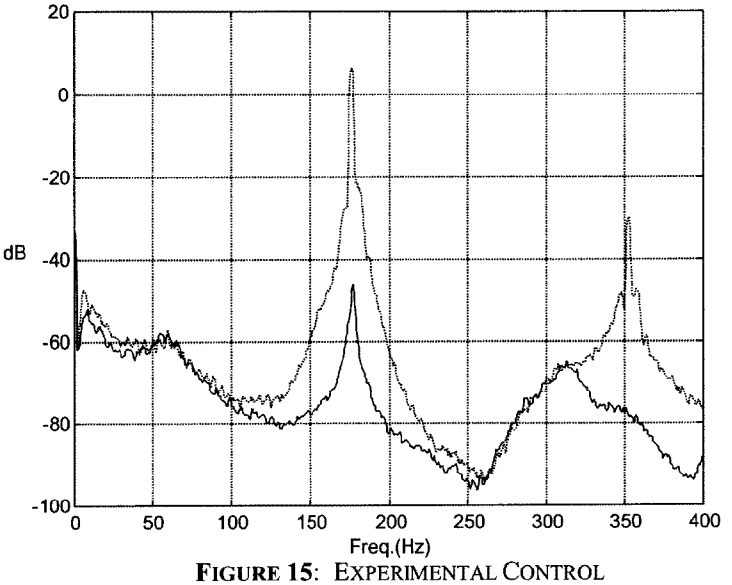

FIGURE 15: EXPERIMENTAL CONTROL

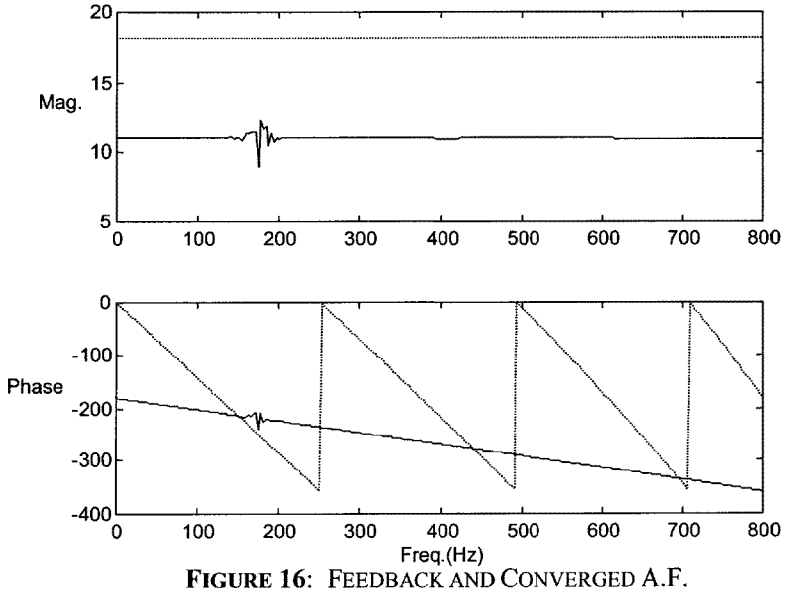

FIGURE 16: FEEDBACK AND CONVERGED A.F.